



RESEARCH ARTICLE

INVESTIGATION OF X-RAY SOURCES IN NGC 7552: IDENTIFICATION OF A NEW ULX CANDIDATE

Sinan ALLAK^{1,*}, Aysun AKYUZ^{1,2}

¹ Space Science and Solar Energy Research and Application Center (UZAYMER), University of Çukurova, 01330, Adana, Turkey
0417allaksinan@gmail.com - [0000-0001-7093-1079](https://orcid.org/0000-0001-7093-1079)

² Department of Physics, University of Çukurova, 01330, Adana, Türkiye
aakyuz@cu.edu.tr - [0000-0001-9533-9805](https://orcid.org/0000-0001-9533-9805)

Abstract

This study investigates the X-ray and optical properties of 29 X-ray sources within the NGC 7552 galaxy, using *Chandra*, Swift X-Ray Telescope (*Swift-XRT*) data, and *Hubble Space Telescope* (*HST*). A significant finding was the identification of a new ultraluminous X-ray source (ULX-3) with an X-ray luminosity, $L_x \approx 10^{39} \text{ erg s}^{-1}$ making it the third ULX identified in this galaxy. The spectral analysis of ULX-3 suggests it could be a stellar-mass black hole with an estimated mass of around 8 solar masses (M_\odot). Nearly half of the observed X-ray binaries (XRBs) were classified as transient or variable. Variability studies revealed that ULX-1 exhibited significant long-term variability in *Chandra* data, while ULX-2 remained stable in both *Chandra* and *Swift-XRT* observations. ULX-3 showed no significant variability in *Chandra* data, indicating steady emissions during the observation period. The analysis of the X-ray energy spectra for ULX-1, ULX-2, and ULX-3 showed that power-law models best described their spectra. These findings suggest that the ULXs have a hard spectral structure, commonly linked to X-ray emissions from compact objects such as black holes or neutron stars. Optical counterparts were also identified for several XRBs, including ULX-1, ULX-2, and ULX-3, most of which exhibit faint optical magnitudes ($m_v > 22 \text{ mag}$) characteristic of ULX systems.

Keywords

Ultraluminous X-ray Sources (ULXs),
X-ray Binaries,
Optical Counterparts of ULXs,
NGC 7552

Time Scale of Article

Received :17 September 2024
Accepted : 02 January 2025
Online date : 25 March 2025

1. INTRODUCTION

X-ray binaries (XRBs) are systems where two stars orbit a common center of mass, consisting of a compact object and a companion star (donor). This compact object can be a neutron star (NS), a black hole (BH), or a white dwarf (WD). XRBs can generally be classified into two different types based on the mass of the donor star: (1) High-mass X-ray binaries (HMXBs, $\geq 10 M_\odot$) and (2) Low-mass X-ray binaries (LMXBs, $\leq 1 M_\odot$). HMXBs typically involve an O or B-type star whose optical/UV brightness is comparable to or greater than that of the X-ray source. The X-ray emission in these systems results from wind accretion, where mass is transferred from the early-type, mass-losing star to the compact star. Additionally, although rare, mass transfer can also occur through Roche lobe overflow in these systems [1]. Furthermore, HMXBs containing an NS may include a Be star (Be/X-ray binary) and a supergiant (SG/X-ray binary). In LMXBs, mass transfer occurs via Roche lobe overflow. Low-mass donor stars can include white dwarfs, late-type main-sequence stars, and F-G-

*Corresponding Author: 0417allaksinan@gmail.com

type subgiants. LMXBs are relatively faint in the optical wavelengths. The emission in the optical region in LMXBs is primarily driven by the radiation from an accretion disk around the compact star. The contribution of the donor star to the emission is generally negligible. In XRBs with an NS, X-ray pulsations can be observed. The NS's strong magnetic field channels the transferred mass to its magnetic poles, creating a bright X-ray hotspot when the mass strikes the hard surface. If the NS's rotational and magnetic axes are not aligned, the emission will be visible once per rotation, resulting in X-ray pulsations. These systems are known as X-ray pulsars. XRBs typically exhibit X-ray luminosities ranging from about 10^{37} – 10^{39} erg/s, depending on the type of system and the characteristics of the compact object. Moreover, some XRBs exhibit much higher luminosities, ranging from 10^{39} – 10^{41} erg/s. These are known as ultraluminous X-ray sources (ULXs).

ULXs are point-like sources located outside the nuclei of their host galaxies, exhibiting X-ray luminosities exceeding 10^{39} erg s^{-1} [2]. ULXs were first discovered in the 1980s by the Einstein Observatory. They began to be better understood with the construction of X-ray observatories with relatively better spectral characteristics, such as *ROSAT*. Recently, next-generation X-ray observatories like *Chandra* and *XMM-Newton* have provided even more information about the spectral and temporal characteristics, and especially the nature, of these sources. Initially, ULXs were thought to be intermediate-mass black holes (IMBHs) with masses in the range of 10^2 - $10^4 M_{\odot}$, assuming their emission and accretion rates were isotropic and limited by Eddington luminosity [3]. Subsequent studies suggested that the primary source of luminosity might be an accretion disk surrounding a compact object in binary systems, potentially exceeding the Eddington limit for X-ray emission [4, 5]. Although there is not yet an identified ULX in our galaxy, Swift J0243.6+6124, which is well-studied and whose compact object has been identified as a neutron star (NS), is a strong candidate for a Galactic ULX.

Theoretical models and population synthesis studies have proposed that the majority of ULXs might contain highly magnetized NSs [6]. They proposed that pulsating ULXs are not strongly beamed, and thus their observed luminosities should be close to their actual luminosities. King et al ([1]) attributed the low number of discovered pulsars ULXs to the fact that magnetic neutron stars emit observable signals only for a short part of their lifetimes. They suggest that a much larger fraction of ULXs, beyond the number of currently discovered pulsar ULXs, may have NS as their compact objects. This interpretation has been reinforced by the discovery of NSs in these systems since 2014 [7], indicating that the ULX population predominantly consists of compact objects accreting at super-Eddington rates [7-12]. Many ULXs can exhibit steady luminosity for several years or even decades. However, some may show significant flux variations on short timescales. Some can completely fade away on the order of days or months and then re-emit at ULX levels [13]. Such sources are called transient ULXs. In some cases, notable flux variability in ULXs can be attributed to the accretion process being halted at the magnetospheric radius of the NS, a phenomenon referred to as the propeller effect [13,14]. Another scenario proposed to explain the variability that these sources may be observed during outbursts of LMXBs [15].

Using ground-based observations and the *Hubble Space Telescope (HST)* along with high-resolution *Chandra* observations, the optical counterparts of ULXs can be determined [13,16]. The emission from the optical counterparts of ULXs may originate from the donor star, the outer part of the accretion disk, or both [17,18]. Photometric and spectroscopic observations allow for detailed characterization of the donor's spectral type, age, metallicity, mass, and the physical conditions of the local environment [19, 20]. ULXs typically have faint optical counterparts (>22 magnitudes). The absolute magnitudes of the identified optical counterparts have been calculated to range between $-4 < M_V < -9$ [21].

The number of identified ULXs continues to grow with new, more sensitive multiwavelength observations. As the ULX population expands, so does the potential to uncover the physical properties

and emission mechanisms of these sources. Our study aims to explore the X-ray population in NGC 7552, with a particular focus on investigating the X-ray and optical properties of ULXs using additional datasets. The enhanced understanding of these features may provide deeper insights into the nature of ULXs, contributing to the broader knowledge of their formation, evolution, and interaction with their host galaxies. NGC 7552 is a starburst ringed, face-on barred spiral galaxy with an inclination of 28 degrees [22]. Throughout this study, the distance to the galaxy NGC 7552, which is morphologically classified as SBbc(s), is assumed to be 19.5 Mpc [23]. Classified mostly as a LINER galaxy [24] this galaxy has not shown significant activity in either X-ray or near-infrared (NIR) band observations of its core [23]. ULX-1 in this galaxy was identified using *ROSAT* observations [25]. Later, using *Chandra* images from 2007, [26] identified ULX-1 and ULX-2 sources, highlighting the bright X-rays. The main objective of this study is to reveal the spectral and temporal properties of the bright X-ray sources within the D_{25} area of the NGC 7552 galaxy using *Chandra* and *Swift-XRT* observations. Additionally, determining their optical counterparts using *HST* archival data and reporting photometric results is another primary goal of this study. For this galaxy, unlike previous studies, more *Chandra* and *Swift-XRT* X-ray observations were used, and for the first time in this study, the properties of the X-ray sources were examined using optical wavelengths.

This paper is organized into three main sections. Section 2 details the reduction and analysis of X-ray and optical data obtained from *Chandra*, *Swift-XRT*, and the *HST*. Section 3 presents the spectral and temporal analysis of 29 X-ray sources in the NGC 7552 galaxy, including a focus on ULX-1, ULX-2, and the newly identified ULX-3, along with their optical counterparts. Finally, Section 4 summarizes the findings, highlighting the new insights gained into the nature and evolution of ULXs.

2. MATERIALS AND METHODS

NGC 7552 has been observed multiple times over 17 years by the *XMM-Newton*, *Chandra*, and *Swift-XRT* X-ray observatories. As shown in Figure 1, *XMM-Newton* observations were excluded due to their insufficient spatial resolution, making it difficult to resolve most sources. Moreover, these observations are affected by high background noise and frequent flaring events. Using *Chandra* observations, 29 X-ray sources have been identified within the D_{25} area. Additionally, different regions of the galaxy have been observed with high-resolution *HST* optical detectors. The *HST*, *Chandra*, and *Swift-XRT* observations used in this study are listed in Table 1. The data reduction and analysis of these observations are detailed in the following sections.

Table 1. X-ray and optical observations of NGC 7552

Instrument	ObsID	Date	Exp. time	
Swift-XRT	46279002	2012-11-07	1.8	
Swift-XRT	46279003	2012-11-08	4.8	
Swift-XRT	46279004	2012-11-10	1.2	
Swift-XRT	46279005	2012-11-11	0.9	
Swift-XRT	46279006	2012-11-16	0.7	
Swift-XRT	46279007	2012-11-18	0.4	
Swift-XRT	46279008	2012-11-20	1.5	
Swift-XRT	46279009	2013-01-07	0.8	
Swift-XRT	10041001	2017-04-04	1.2	
Swift-XRT	10041002	2017-04-08	1.9	
Swift-XRT	10041003	2017-04-12	0.8	
Swift-XRT	10041004	2017-04-16	1.5	
Swift-XRT	10041005	2017-04-20	0.7	
Swift-XRT	10041006	2017-04-21	1.1	
Swift-XRT	10041007	2017-04-23	1.8	
Swift-XRT	10041008	2017-04-29	1.6	
Swift-XRT	10041009	2017-05-06	1.4	
Swift-XRT	10041010	2017-05-10	0.5	
Swift-XRT	3104723001	2018-06-06	0.4	
Swift-XRT	3104723004	2018-07-18	1.6	
Swift-XRT	88883001	2018-07-18	2.2	
Chandra/ACIS-S	7848	2007-03-31	5.0	
Chandra/ACIS-S	20268	2018-08-20	12.0	
Chandra/ACIS-S	20267	2018-08-21	57.0	
Chandra/ACIS-S	21675	2018-08-24	65.0	
Chandra/ACIS-S	21676	2018-08-24	66.0	
				Filter
HST/WFPC2	ubah3301m	2009-05-05	60.5	F439W
HST/WFPC2	ubah330bm	2009-05-05	65.6	F555W
HST/WFPC2	ubah330cm	2009-05-05	65.6	F814W

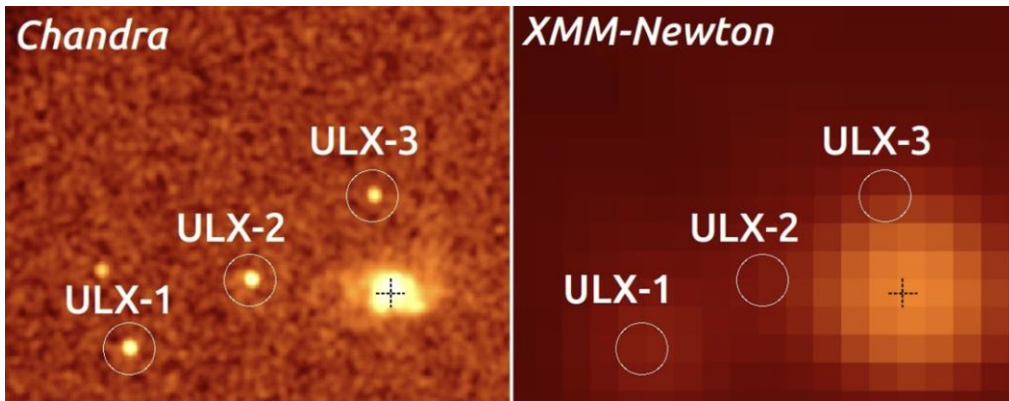


Figure 1. A detailed view of the ULX positions on *Chandra* (left) and *XMM-Newton* (right) images.

2.1. X-ray Data Reduction and Analysis

Chandra ACIS-S observations were analyzed using the *Chandra Interactive Analysis of Observations* (CIAO) v4.14 software and calibration files *CALDB* v4.9.6. The observation files were prepared for analysis using the *CIAO chandra_repro* packages. Using *Chandra* data, 29 X-ray sources were identified within the D_{25} area. The right panel of Figure 2 shows these sources on the X-ray RGB (Red: Green: Blue) image. The sources were numbered in ascending order of *Chandra* cumulative counts. Spectral, temporal, and statistical (photon count rate) analyses were performed by selecting both the source and background regions using circles with a radius of 5 arcseconds (")

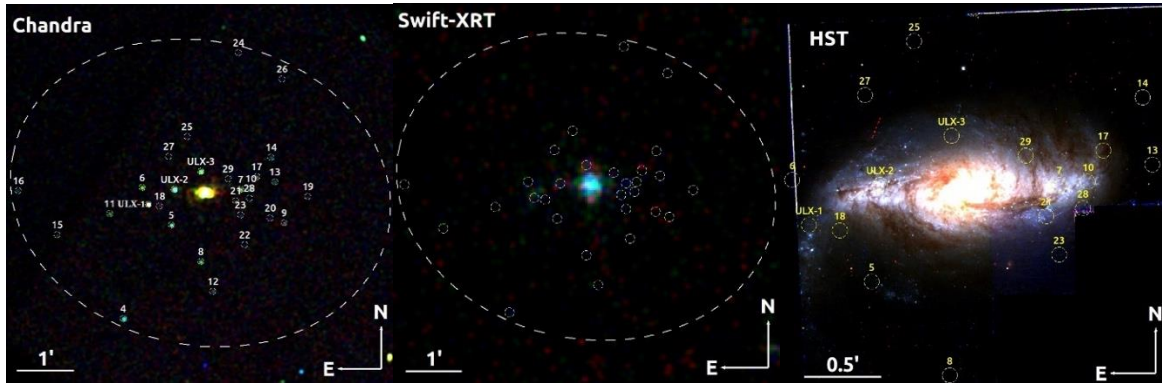


Figure 2. Three-color (RGB, R: red; G: green; B: blue) images of the NGC 7552 galaxy from *Chandra* (Observation ID 21676) (left), *Swift-XRT* (a combination of 2012 observations) (center), and HST (right). The *Chandra* and *Swift-XRT* RGB images were created using energy bands of 0.3-1 keV, 1-2 keV, and 2-8 keV, respectively, while the HST RGB image was composed using the F814W, F555W, and F435W filters. The large dashed ellipse represents the D_{25} region, and the smaller dashed hollow circles indicate the positions of the X-ray sources.

Source spectra and light curves were obtained using the *specextract* and *dmextract* packages, respectively. Additionally, spectra from 2018 *Chandra* data with closely spaced observation dates were combined using the *combine_spectra* package. This process enabled the analysis of the spectral and temporal properties of faint sources with low photon counts.

Spectral analyses were performed using the *XSPEC* v12.8.2 software. Based on the total source counts, the source energy spectra were grouped with a minimum of 10 counts per energy bin. Count rates and spectra for all detectors were obtained in the 0.3-10 keV energy range. Fundamental models for XRBs, such as the power-law and *diskbb* models, were applied to the source spectra. Additionally, combined models like the power-law+*diskbb* model were also applied. An absorption column component (TBABS) was included in these models.

Photon count rates for *Swift-XRT* in PC (Photon Counting) mode were obtained using the automated procedures specified on the website [27]. Due to the typically short exposure time of *Swift-XRT* observations, the data are statistically insufficient for model application. Therefore, *Swift-XRT* observations were used only for temporal analyses in this study.

The short-term and long-term characteristics of X-ray sources provide significant insights into their nature. Some sources can exhibit flux variations of more than 50 times over the long term [13]. These variations can provide crucial insights into the types of compact objects they contain. For instance, the high flux variations observed in pulsar ULXs typically display a bi-modal distribution. This is often an indication of a mechanism known as the propeller effect [28, 29]. This effect occurs directly when the compact objects are NSs. Additionally; short-term variations are examined for pulsar-like signals or quasi-periodic oscillations (QPO). These analyses can also indicate of whether the compact object is a

neutron star or a black hole. In this study, short-term and long-term flux variations were examined to investigate such characteristics of X-ray sources.

For short-term analyses, light curves were produced using *Chandra* datasets cleaned from the background in the 0.3-10 keV energy range. For long-term light curves, count rates ($count\ s^{-1}$) from *Chandra* and *Swift-XRT* observations in the 0.3-10 keV energy range were used. Long-term variations were calculated using the 2007 and combined 2018 *Chandra* observations. The variability of the sources was calculated using *Chandra* data, owing to its superior pixel resolution. Based on these two datasets, X-ray sources were classified as variable if the variation factor (V_f), defined as the ratio of the highest flux to the lowest flux, was ≥ 3 . Table 2 shows the X-ray sources identified within the D_{25} region of the NGC 7552, along with their coordinates in degrees and their variation factors. Moreover, long-term variations of sources, including ULXs, were examined using *Swift-XRT* observations. However, light curves for all sources were not generated, as not all sources were resolved by the *Swift-XRT* detector and/or due to their transient nature. High-quality observations with strong data statistics are particularly needed to investigate pulsar-like strong signals.

Table 2. The X-ray sources located within the D_{25} region of the NGC 7552 are described by their coordinates, fluxes (F_X), and variability factors (V_f).

Source No.	RA	Decl.	F_X	V_f
	($^{\circ}$)	($^{\circ}$)	($10^{-14} erg\ cm^{-2}\ s^{-1}$)	(T=Transit)
ULX-1	349.0674	-42.5884	6.2 ± 0.1	4.1
ULX-2	349.0569	-42.5840	10.2 ± 0.1	1.2
ULX-3	349.0463	-42.5787	2.22 ± 0.01	1.8
X4	349.0774	-42.6222	1.42 ± 0.4	1.2
X5	349.0581	-42.5945	0.91 ± 0.3	1.3
X6	349.0699	-42.5835	0.71 ± 0.3	1.7
X7	349.0304	-42.5840	0.68 ± 0.2	T
X8	349.0464	-42.6054	0.62 ± 0.2	1.1
X9	349.0129	-42.5940	0.48 ± 0.2	T
X10	349.0262	-42.5837	0.46 ± 0.2	1.4
X11	349.0830	-42.5912	0.41 ± 0.1	1.6
X12	349.0415	-42.6142	0.37 ± 0.1	T
X13	349.0167	-42.5818	0.34 ± 0.2	T
X14	349.0181	-42.5745	0.34 ± 0.1	1.7
X15	349.1040	-42.5974	0.32 ± 0.1	2.5
X16	349.1196	-42.5844	0.31 ± 0.1	2.8
X17	349.0239	-42.5803	0.28 ± 0.1	1.2
X18	349.0628	-42.5890	0.22 ± 0.1	T
X19	349.0033	-42.5861	0.18 ± 0.1	2.5
X20	349.0184	-42.5925	0.17 ± 0.01	1.6
X21	349.0323	-42.5874	0.15 ± 0.01	1.5
X22	349.0288	-42.6004	0.15 ± 0.01	3.4
X23	349.0304	-42.5916	0.15 ± 0.01	2.3
X24	349.0312	-42.5435	0.13 ± 0.01	T
X25	349.0518	-42.5684	0.13 ± 0.01	T
X26	349.0137	-42.5514	0.11 ± 0.01	T
X27	349.0591	-42.5743	0.10 ± 0.01	1.2
X28	349.0269	-42.5866	0.07 ± 0.01	4.7
X29	349.0354	-42.5809	0.07 ± 0.01	1.1

However, to examine short-term count rates, background-subtracted Chandra light curves were produced in the 0.3-10 keV energy range with time intervals of 3.14 seconds. No sources showing significant short-term variations were found. To gain further insights into the nature of all these sources, new observations with high data statistics are required.

2.2. Optical Data Reduction and Analysis

NGC 7552 was observed by *HST* in 2009 using *WFPC2/WFC* (*The Wide Field and Planetary Camera 2/ The Wide Field Camera*). In this study, the F439W, F555W, and F814W filters were utilized. The details of the observations are provided in Table 1. High-resolution *Chandra* and *HST* images are frequently used to identify the optical counterparts of XRBs. However, none of the X-ray sources in the NGC 7552 galaxy matched any sources identified in the *HST* optical images. Therefore, relative astrometry was indirectly performed between *Chandra* and *HST* using the *GAIA R2* optical catalog. Two reference sources were identified between *Chandra* and *GAIA*. Using these reference sources, errors for right ascension (*R.A*) and declination (*Decl.*) were determined between the two images. These errors are defined based on the standard deviation calculation using the offsets between the reference sources. Subsequently, 10 reference sources were selected between *GAIA* and *HST*, and errors were calculated for *R.A* and *Decl.*, respectively.

Astrometric calculations were performed following the method from our previous studies [30]. As a result, the optical coordinates and errors of the X-ray sources were calculated. *Chandra* (5932) and *HST WFPC2/WFC* (F555W) images were used for astrometric corrections. Sources were identified using the *wavedetect* and *IRAF/daofind* packages. All identified reference sources are shown in Figure 3. The root mean square of the total errors between *Chandra* and *GAIA* and between *GAIA* and *HST* provides an astrometric error radius of 0.34" with 90% confidence. Within the astrometric error radius, only the sources X8, X16, X17, ULX-1, ULX-2, and ULX-3 were found to have optical counterparts.

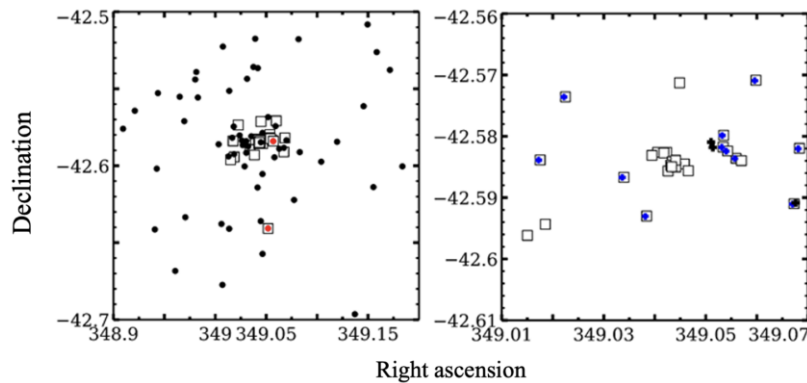


Figure 3. Left panel: The coordinates of *Chandra* and *GAIA* sources are represented by filled circles and hollow squares, respectively. The references between *Chandra* and *GAIA* are shown as red filled circles. Right panel: The coordinates of *GAIA* and *HST* sources are represented by hollow squares and dark crosses, respectively. The reference sources between these two images are represented by blue crosses.

The photometric analyses of these optical counterparts were performed using the *APPHOT* package in the *IRAF* software. Circles with radii of 3 and 12 pixels were selected for the source and background, respectively. Aperture correction was also carried out for each filter using 25 isolated and bright sources with radii ranging from 3 pixels to 24 pixels. Accordingly, the aperture corrections for the F439W (B), F555W (V), and F814W (I) filters were calculated as -0.32, -0.28, and -0.24 magnitudes, respectively. The resulting magnitudes were then corrected for extinction (A_V) using a value of $A_V = 0.04$ magnitudes from the study by [31]

Color-magnitude diagrams (CMDs) of $F439W-F555W$ versus $F555W$ and $F555W-F814W$ versus $F814W$ were generated to estimate the ages and masses of the optical counterparts [36]. *PARSEC* isochrones were employed in the CMDs. The metallicity and distance modulus of NGC 7552 were set to solar metallicity ($Z = 0.02$) and 31.45 magnitudes, respectively, for CMD construction. The *PARSEC* isochrones were corrected with an extinction value of $A_V = 0.04$. In generating the CMDs, it was assumed that the optical emission originated entirely from the donor star.

3. RESULTS AND DISCUSSION

3.1. X-ray

The X-ray and optical properties of the X-ray sources within the NGC 7552 galaxy have been investigated using *Chandra*, *Swift-XRT*, and *HST* data spanning over 17 years. Using *Chandra* data, 29 X-ray sources were identified within the D_{25} . These sources do not correspond to any cataloged AGN, background galaxy, or foreground star. All sources, including the previously identified ULX-1 and ULX-2, were analyzed using *Chandra* and *Swift-XRT* archival data sets. The previously identified ULX-1 and ULX-2 in the NGC 7552 galaxy were examined using combined *Chandra* spectra from the studies of [25, 26] which utilized *ROSAT* and 2007 *Chandra* data. The luminosity values for these sources are nearly identical to those calculated in this study. Although study [26] used a distance of 21.6 Mpc for the NGC 7552 galaxy, compared to 19.5 Mpc here, the results remain consistent. This similarity can be attributed to the combination of 2018 *Chandra* spectra, which improved the data statistics with a total observation time of 200 ks. The *power-law* model parameters and luminosity values that best represent the spectra of these two sources are shown in Table 3. Throughout this study, models with a reduced chi-square (χ^2) value of 0.75-1.50 were considered the best fits. The photon indices (Γ) of ULX-1 and ULX-2, 1.8 and 2.4 respectively, are consistent with a hard state characterized by non-thermal emission [32-35].

One of the most significant outcomes of this study is the identification of a third ULX candidate in the NGC 7552 galaxy. In previous studies [26], the luminosity values of source X17 (hereafter referred to as ULX-3) were calculated to be below the ULX level of luminosity. Using the combined 2018 *Chandra* spectrum and the best-fitting *power-law* model, its luminosity in the 0.3-10 keV range has been calculated to be $L_X = 1.1 \times 10^{39} \text{ erg s}^{-1}$. This value classifies this source a ULX candidate. The *power-law* model parameter that best represents its energy spectrum was calculated as $\Gamma=1.9$ (see Table 3). Assuming accretion at Eddington luminosities, the compact object's mass was found to be $\sim 8M_\odot$, indicating a stellar-mass black hole. Figure 4 shows the energy spectra of ULX-1, 2, and 3 fitted with the *power-law* model.

Table 3. *Power-law* model parameters that best represent the energy spectra of the ULX candidates.

Source	N_H	N_p	Γ	F_X	L_X	χ^2/dof
	10^{22}	10^{-5}		10^{-14}	10^{39}	
ULX-3	4.5 ± 0.4	3.8 ± 1.6	1.9 ± 0.5	2.2 ± 0.1	1.1 ± 0.1	28.2/30
ULX-2	0.2 ± 0.0	1.6 ± 0.4	1.8 ± 0.2	10.2 ± 0.1	4.6 ± 0.1	62.2/85
ULX-1	0.1 ± 0.0	1.3 ± 0.2	2.4 ± 0.3	6.4 ± 0.1	2.9 ± 0.2	64.6/64

Note. N_H : Intrinsic X-ray absorption value in units of 10^{22} cm^{-2} . N_p : Normalization parameter of *power-law* model in units of 10^{-5} . Γ is the photon index from the *power-law* model. F_X is unabsorbed fluxes in units of $10^{-13} \text{ erg cm}^{-2} \text{ s}^{-1}$. L_X is unabsorbed luminosities in units of $10^{39} \text{ erg s}^{-1}$ in the 0.3–10 keV energy range. χ^2/dof is the reduced. All errors are at the 90% confidence level.

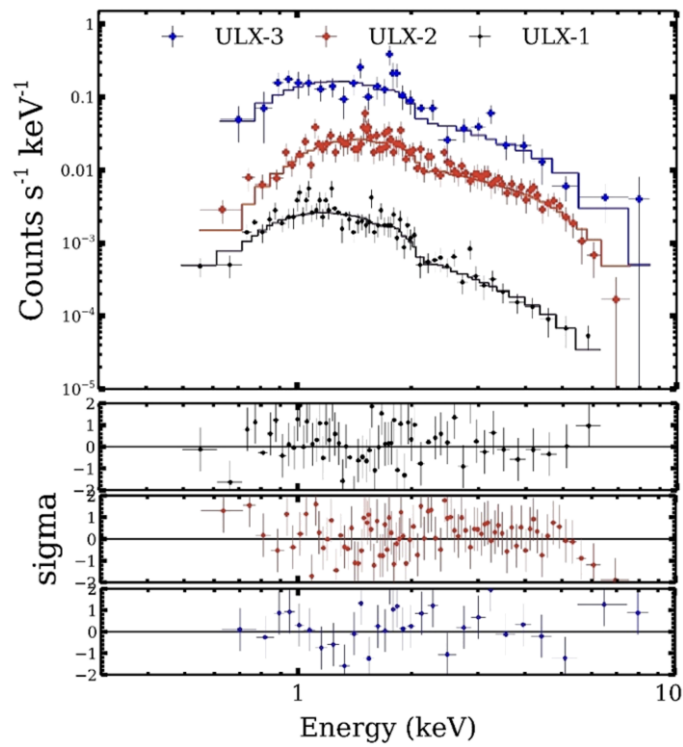


Figure 4. Energy spectra of three ULX candidates located in the NGC 7552 galaxy: ULX-3 (dark blue crosses), ULX-2 (dark red crosses), and ULX-1 (black crosses). The residuals from the fitting process are displayed in the bottom panels (data-model)/error.

Variability factors (V_f) were calculated using 2007 and combined 2018 *Chandra* data. Sources were defined as a variable when the variability factor $V_f \geq 3$ and sources detected in one observation but not in another were defined as transient (see Table 2). Accordingly, sources X16, X22, X28 and ULX-1 were considered variable. Additionally, X7, X9, X12, X13, X18, X24, X25, and X26 sources which were not detected in the 2007 *Chandra* data but were detected in the 2018 images, were defined as transient sources. Two of the three ULXs, ULX-2, and ULX-3, do not show any variability in long-term *Chandra* data. The long-term variability of the variable and transient sources, including the ULX candidates, was also investigated using *Swift-XRT* observations.

None of the transient sources were detected in any of the *Swift-XRT* observations. This could be due to the observations not having sufficiently long exposure times to detect these faint sources, or because their transient nature means they may have prevented them from emitting during these periods. Light curves created based on the count rate for sources ULX-1, ULX-2, ULX-3, X4, and X28 using *Swift-XRT* observations are shown in Figure 5. ULX-1 and ULX-2 did not show strong variability ($V_f \leq 3$) in the *Swift-XRT* observations. In contrast, ULX-3 which did not show significant variability in *Chandra* observations exhibited variability ($V_f \sim 6$) in *Swift-XRT* observations. X24 maintained its variable nature, while no significant changes were observed for X28 in these observations. Variable sources can remain constant during some periods.

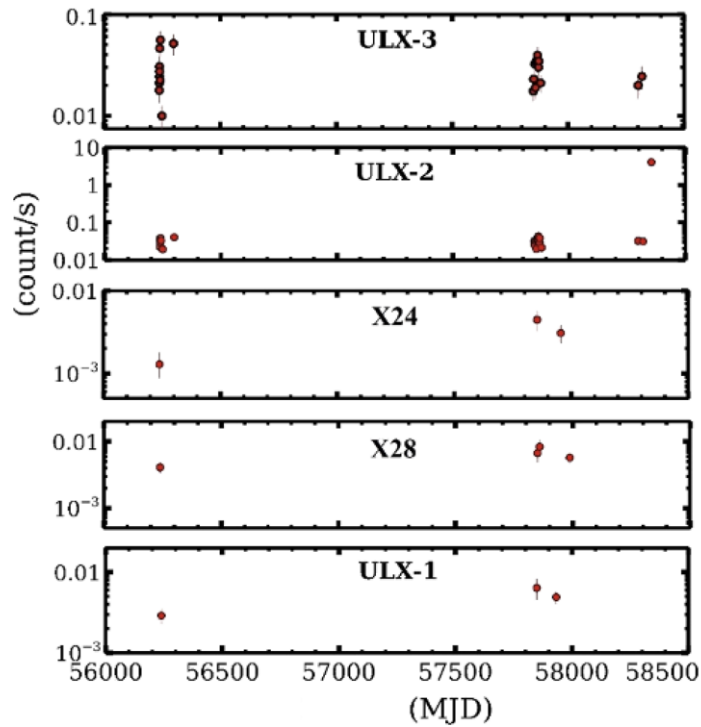


Figure 5. Long-term X-ray light curves of variable sources and those classified as ULX candidates were obtained using *Swift-XRT* observations.

3.2. Optical

Based on advanced astrometry from *Chandra*, *GAIA*, and *HST* observations, potential optical counterparts for the X-ray sources were identified. By examining the optical images listed in Table 1, optical counterparts for ULX-1, ULX-2, ULX-3, X5, X8, X13, X14, X21, and X29 were identified within an astrometric error radius of 0.34" with 90% confidence level. No optical counterparts were found within the astrometric error radius for the remaining sources. Figure 6 shows the position of the optical counterpart of ULX-3 on the *HST* image. Table 4 provides the coordinates and Vega magnitudes in three filters for the sources with identified optical counterparts.

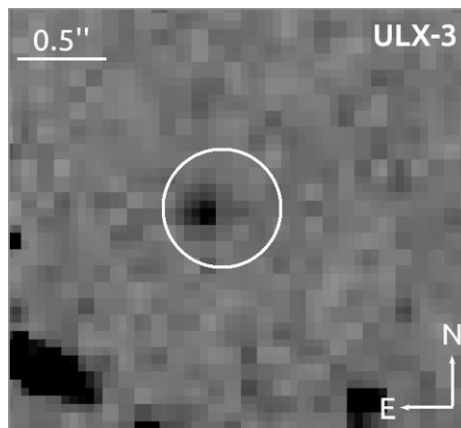


Figure 6. The optical counterpart of ULX-3 is shown on the *HST* F439W image. The solid white circle represents the astrometric error region with a radius of 0.34".

Table 4. The counterparts and their Vega magnitudes in three filters.

Filter/source	F439W	F555W	F814W
ULX-1	22.6 ± 0.4	22.20 ± 0.2	21.9 ± 0.3
ULX-2	19.8 ± 0.2	19.6 ± 0.2	19.4 ± 0.2
ULX-3	22.3 ± 0.3	...	21.5 ± 0.4
X5	24.8 ± 0.6
X8	23.4 ± 0.4	...	23.3 ± 0.5
X13	25.1 ± 0.7	24.2 ± 0.4	21.9 ± 0.2
X14	25.3 ± 0.6	23.5 ± 0.5	24.2 ± 0.5
X21	22.9 ± 0.7	22.8 ± 0.4	22.8 ± 0.7
X29	22.5 ± 0.5

All sources with identified optical counterparts must have sufficiently distinct and bright donor stars, as they were detected in at least one *HST* filter. For NGC 7552, at a distance of 19.5 Mpc, the lower detection limit for donor stars of XRBs in *HST* observations is likely greater than $8 M_{\odot}$, which is the lowest mass calculated for the optical sources. This suggests that the sources can be classified as HMXBs. The lack of optical counterparts for the other sources is likely due to their faintness and small donor mass, suggesting they could be LMXBs [37]. On the other hand, analyses of James Webb Space Telescope observations have provided clues indicating that the donor stars of ULXs without identified optical counterparts may be embedded in dense, hot gas and dust [38-40]. Consecutive optical observations in different filters will provide critical insights into the optical emission mechanisms through analyses of optical temporal variability and spectral energy distributions. These observations will help determine whether the optical emission originates from the accretion disk, the donor star, or both.

The apparent magnitudes in the V-band (F555W) indicate that most ULX optical counterparts are faint, similar to other ULX counterparts [16-18]. The CMDs showing the ages and masses of the optical counterparts of ULXs, X14, and X21 are presented in Figure 7. These diagrams shows that the probable masses of the optical counterparts range from 8 to $30 M_{\odot}$, with ages between 4 and 20 Myr.

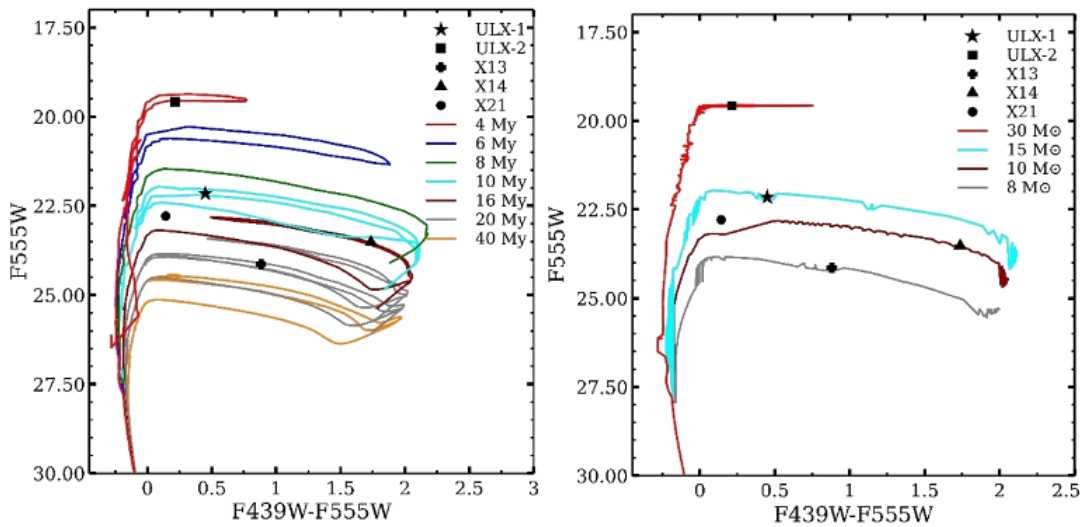


Figure 7. Color-magnitude diagrams (CMDs) of the identified optical counterparts of ULXs and XRBs. PARSEC isochrones of different ages (left panel) and masses (right panel) are overlotted. Isochrones have been corrected with an $A_V=0.04$ value.

4. CONCLUSION

Previous X-ray studies of the galaxy NGC 7552 have identified numerous bright X-ray sources, including ULX-1 and ULX-2 [26]. However, detailed analyses of other faint sources have not been conducted. In contrast, this study provides a thorough spectral and temporal analysis of 29 X-ray sources within the D25 field of the galaxy, utilizing a broader range of archival data. Our main findings are summarized as follows:

I. This study has provided a detailed analysis of the X-ray and optical properties of 29 XRBs within the NGC 7552 galaxy, leading to the discovery of a new ultraluminous X-ray source (ULX-3). This identification contributes to the growing understanding of X-ray sources within this galaxy.

II. Analysis of the energy spectrum suggests that ULX-3 is likely a stellar-mass black hole with an estimated mass of around $8 M_{\odot}$. This supports the hypothesis that ULX-3 is a compact stellar-mass object exhibiting high-energy X-ray emissions.

III. ULX-1 exhibited significant long-term variability in *Chandra* data, indicating dynamic changes in its flux over time. In contrast, ULX-2 showed no significant variability in either *Chandra* or *Swift-XRT* observations, maintaining a stable luminosity throughout. Similarly, ULX-3 did not exhibit variability in *Chandra* data but displayed significant variability in *Swift-XRT* observations, suggesting that its variability may manifest over shorter timescales.

IV. Nearly 50% of the identified X-ray sources are either transient or variable. This finding suggests that the population of XRBs or ULXs appears to grow as galaxies are re-observed and re-examined.

V. Optical counterparts were identified for ULX-1, ULX-2, and ULX-3. These counterparts are consistent with the faint optical characteristics commonly associated with ULX systems. Therefore, high-quality, long-term, and simultaneous multiwavelength observations will be crucial for better understanding the emission mechanisms, particularly in determining whether the emission primarily originates from the donor star or other components such as the accretion disk. Such observations will also help refine the variability characteristics and physical properties of these ULXs, leading to a more comprehensive understanding of their nature.

ACKNOWLEDGEMENTS

This paper was supported by the Scientific and Technological Research Council of Türkiye (TÜBİTAK) through project number 122C183.

CONFLICT OF INTEREST

The author(s) stated that there are no conflicts of interest regarding the publication of this article.

CRedit AUTHOR STATEMENT

Sinan Allak: Formal analysis, Writing – original draft, Visualization. **Aysun Akyuz:** Supervision, Project administration, Conceptualization.

REFERENCES

- [1] Lewin WHG, van Paradijs J, van den Heuvel EPJ. X-ray Binaries. Cambridge University Press 1997: 674.

- [2] King A, Lasota, J.-P, and Middleton M, Ultraluminous X-ray sources. *New Astronomy Reviews* vol. 2023; 96: 101672.
- [3] Colbert EJM, Mushotzky RF. The nature of accreting black holes in nearby galaxy nuclei *The Astrophysical Journal*, 1999; 519: 89.
- [4] Begelman MC. Super-Eddington Fluxes from Thin Accretion Disks? *The Astrophysical Journal* 2002; 568(2): L97–L100.
- [5] Walton DJ. A Potential Cyclotron Resonant Scattering Feature in the Ultraluminous X-Ray Source Pulsar NGC 300 ULX1 Seen by NuSTAR and XMM-Newton. *The Astrophysical Journal* 2018; 857(1): L3.
- [6] Mushtukov AA, Suleimanov VF, Tsygankov SS, Poutanen J. On the maximum accretion luminosity of magnetized neutron stars: connecting X-ray pulsars and ultraluminous X-ray sources. *MNRAS* 2015; 454(3): 2539–2548.
- [7] Bachetti M. An ultraluminous X-ray source powered by an accreting neutron star. *Nature*, 2014; 514(521): 202–204.
- [8] Fürst F. Discovery of Coherent Pulsations from the Ultraluminous X-Ray Source NGC 7793 P13. *The Astrophysical Journal* 2016; 831(2): L14.
- [9] Israel GL. An accreting pulsar with extreme properties drives an ultraluminous x-ray source in NGC 5907. *Science* 2017; 355(6327): 817–819.
- [10] Carpano S, Haberl F, Maitra C, Vasilopoulos G. Discovery of pulsations from NGC 300 ULX1 and its fast period evolution. *MNRAS* 2018; 476(1): L45–L49.
- [11] Sathyaprakash R. The discovery of weak coherent pulsations in the ultraluminous X-ray source NGC 1313 X-2. *MNRAS* 2019; 488(1): L35–L40.
- [12] Rodríguez Castillo GA. Discovery of a 2.8 s Pulsar in a 2 Day Orbit High-mass X-Ray Binary Powering the Ultraluminous X-Ray Source ULX-7 in M51. *The Astrophysical Journal* 2020; 895(1): 60.
- [13] Allak S. The transient ultraluminous X-ray source, ULX-4, in M51. *MNRAS* 2022; 510(3): 4355–4369.
- [14] Erkut MH, Ekşi KY, Alpar MA. Ultra-luminous X-Ray Sources as Super-critical Propellers. *The Astrophysical Journal* 2019; 873(2): 105.
- [15] Earnshaw HP, Roberts TP, Sathyaprakash R. Searching for propeller-phase ULXs in the XMM-Newton Serendipitous Source Catalogue. *MNRAS* 2018; 476(3): 4272–4277.
- [16] Allak S. Detection of 125.5-day optical periodic modulation of the neutron star M51 ULX-8. *MNRAS* 2022; 517(3): 3495–3504.
- [17] Tao L, Feng H, Grisé F, Kaaret P. Compact Optical Counterparts of Ultraluminous X-Ray Sources. *The Astrophysical Journal* 2011; 737(2): 81.

- [18] Gladstone JC. Optical Counterparts of the Nearest Ultraluminous X-Ray Sources. *The Astrophysical Journal Supplement Series* 2013; 206(2): 14.
- [19] Kaaret P, Ward MJ, Zezas A. High-resolution imaging of the HeII λ 4686 emission line nebula associated with the ultraluminous X-ray source in Holmberg II. *MNRAS* 2004; 351(3): L83–L88.
- [20] Grisé F, Kaaret P, Corbel S, Feng H, Cseh D, Tao L. Optical Emission of the Ultraluminous X-Ray Source NGC 5408 X-1: Donor Star or Irradiated Accretion Disk? *The Astrophysical Journal* 2012; 745(2): 123.
- [21] Vinokurov A, Fabrika S, Atapin K. Optical Counterparts of Ultraluminous X-Ray Sources NGC 4559 X-10 and NGC 4395 ULX-1. *The Astrophysical Journal* 2018; 854 (2): 176.
- [22] Schinnerer E. The Circumnuclear Starburst in NGC 7552: First Results from Near-Infrared Spectral Synthesis. *The Astrophysical Journal* 1997; 488 (1): 174–194.
- [23] Tully RB, Fisher JR. Book-Review - Nearby Galaxies Atlas. *Science* 1988; 239: 926.
- [24] Durret F, Bergeron J. Long slit spectroscopy of emission line galaxies. I. The sample. *Astronomy and Astrophysics Supplement Series* 1988; 5: 273–297.
- [25] Liu JF, Bregman JN. Ultraluminous X-Ray Sources in Nearby Galaxies from ROSAT High Resolution Imager Observations I. Data Analysis. *The Astrophysical Journal Supplement Series* 2005; 157(1): 59–125.
- [26] Luangtip W. A deficit of ultraluminous X-ray sources in luminous infrared galaxies. *MNRAS* 2015; 446(1): 470–492.
- [27] Evans PA. Methods and results of an automatic analysis of a complete sample of Swift-XRT observations of GRBs. *MNRAS* 2009; 397(3): 1177–1201.
- [28] Tsygankov SS, Mushtukov AA, Suleimanov VF and Poutanen J. Propeller effect in action in the ultraluminous accreting magnetar M82 X-2. *MNRAS* 2016; 457(1): 1101–1106.
- [29] Song X. The hunt for pulsating ultraluminous X-ray sources. *MNRAS* 2020; 491(1): 1260–1277.
- [30] Allak S. Detection of 125.5-day optical periodic modulation of the neutron star M51 ULX-8. *MNRAS* 2022; 517(3): 3495–3504.
- [31] Schlafly EF and Finkbeiner DP. Measuring Reddening with Sloan Digital Sky Survey Stellar Spectra and Recalibrating SFD. *The Astrophysical Journal* 2011; 737(2): 103
- [32] Remillard RA and McClintock JE. X-Ray Properties of Black-Hole Binaries. *Annual Review of Astronomy and Astrophysics* 2006; 44(1): 49–92.
- [33] Feng H, Kaaret P. Spectral States and Evolution of Ultraluminous X-Ray Sources. *The Astrophysical Journal* 2009; 696(2): 1712–1726.
- [34] Jin J, Feng H, Kaaret P. Transition to the Disk Dominant State of a New Ultraluminous X-ray Source in M82. *The Astrophysical Journal* 2010; 716(1): 181–186.

- [35] Koliopoulos F, Vasilopoulos G, Buchner J, Maitra C, Haberl F. Investigating ULX accretion flows and cyclotron resonance in NGC 300 ULX1. *Astronomy and Astrophysics* 2019; 621.
- [36] Bressan A. PARSEC: stellar tracks and isochrones with the PAdova and TRieste Stellar Evolution Code. *MNRAS* 2012; 427(1): 127–145.
- [37] Hunt Q. Calibrating X-Ray Binary Luminosity Functions via Optical Reconnaissance. I. The Case of M83. *The Astrophysical Journal* 2021; 912(1): 31.
- [38] Allak S. Comprehensive X-ray and multiwavelength study of ULXs in NGC 1566. *MNRAS* 2024; 527(3): 556–7567.
- [39] Allak S. The first glimpse of ULXs through the near-infrared images captured by the JWST. *MNRAS* 2024; 527(2): 2599–2611.
- [40] Allak S. New transient ULX candidate in NGC 4254: evidence of circumbinary disc? *MNRAS* 2023; 526(4): 5765–5776.